IOP Conf. Series: Journal of Physics: Conf. Series **807** (2017) 052010 doi:10.1088/1742-6596/807/5/052010

Vortex states in a superconductor under a helical magnetic field

Saoto Fukui[1], Masaru Kato[1] and Yoshihiko Togawa[2]

[1] Department of Mathematical Sciences, Osaka Prefecture University, 1-1, Gakuencho, Nakaku, Sakai, Osaka 599-8531, Japan

[2] Department of Physics and Electronics, Osaka Prefecture University, 1-1, Gakuencho, Nakaku, Sakai, Osaka 599-8531, Japan

E-mail: st110035@edu.osakafu-u.ac.jp

Abstract. We have studied vortex states in a chiral helimagnet / superconductor bilayer system numerically. We consider a two-dimensional superconductor subsystem. An effect of a chiral helimagnet on a superconductor is taken as a magnetic field, which oscillates spatially. Solving the Ginzburg-Landau equations, we obtain various vortex states. Comparing free energies, we find the most stable vortex states under only the oscillating magnetic field $H_{\rm CHM}$ and under the $H_{\rm CHM}$ and the homogeneous applied magnetic field $H_{\rm appl}$.

1. Introduction

Recently, a chiral helimagnet (CHM) attracts attention in the field of magnetism [1]. This magnetic structure consists of spins that form a helical rotation along a helical axis in Fig.1(a). In the CHM, there are two interactions between nearest neighbor spins; a ferromagnetic exchange interaction and the Dzyaloshinsky-Moriya (DM) interaction[2, 3]. The ferromagnetic interaction causes nearest neighbor spins to be parallel. On the other hand, the DM interaction causes nearest neighbor spins to be perpendicular to each other. The competition between two interactions leads to the small finite angle between nearest neighbor spins. Then, all spins rotates along the helical axis. Under an applied magnetic field, this helical magnetic structure in the CHM changes into a chiral soliton lattice (CSL), which consists of ferromagnetic domains periodically partitioned by 360° domain walls in Fig.1(b). We can regard domain walls as solitons. In the experiment, the magnetic structure of the CHM and the CSL are observed recently[1].

We focus on the effect of the chiral helimagnet on a superconductor(SC). In general, there appear vortices in type-II SCs under a homogeneous magnetic field. These vortices are affectied by the strength of the magnetic field and external current. Also, vortices are affected by a ferromagnet(FM). The FM / SC hybrid structure enhances critical current because of a pinning of vortices[4]. We expect that the CHM also affects vortices strongly. The helical magnetic structure of the CHM causes a helical magnetic field outside the CHM. So, we investigate vortex states in the SC under the helical magnetic field. For this purpose, we solve the Ginzburg-Landau equations numerically[5, 6, 7], and obtain stable vortex states.

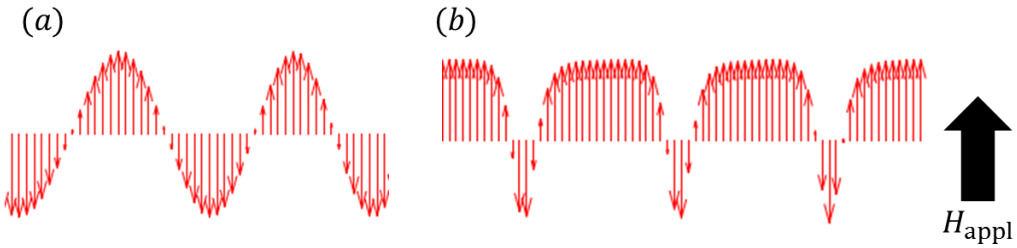

Figure 1. Spin configurations of (a) a chiral helimagnetic structure, and (b) a chiral soliton lattice under an applied magnetic field $H_{\rm appl}$.

2. Methods

We consider a CHM / SC bilayer system in Fig.2. First, we neglect effects of the SC on the CHM. On the other hand, the effect of the CHM on SC is taken as an external magnetic field $\boldsymbol{H}_{\rm CHM}$. We assume the distribution of $\boldsymbol{H}_{\rm CHM}$ is same as the spin configuration of the CHM. So, $\boldsymbol{H}_{\rm CHM}$ is helical along the helical axis. We consider a two-dimentional SC system. Then, only the perpendicular component of $\boldsymbol{H}_{\rm CHM}[(\boldsymbol{H}_{\rm CHM})_z]$ can be taken into account. Since $(\boldsymbol{H}_{\rm CHM})_z$ oscillates spatially, this situation is same as the two-dimenstional SC system under the oscillating magnetic field $(\boldsymbol{H}_{\rm CHM})_z$. $\boldsymbol{H}_{\rm CHM}$ is obtained from a Hamiltonian for the CHM[8];

$$\mathcal{H} = -J\sum_n \boldsymbol{S}_n \cdot \boldsymbol{S}_{n+1} + \boldsymbol{D}\cdot\sum_n \boldsymbol{S}_n \times \boldsymbol{S}_{n+1} + 2\mu_B \boldsymbol{H}_{\rm appl}\sum_n \boldsymbol{S}_n^z, \tag{1}$$

where S_n is a n-th spin, μ_B is the Borh magneton, $\boldsymbol{H}_{\rm appl} = (0, 0, H_{\rm appl})$ is the homogeneous applied magnetic field, J is the coefficient of the exchange interaction, and $\boldsymbol{D} = (D, 0, 0)$ is a DM vector that is parallel to the helical axis. The spin is expressed in a polar coordinate;

$$\boldsymbol{S}_n = S(\sin\theta_n\cos\phi,\ \ \sin\theta_n\sin\phi, \cos\theta_n). \tag{2}$$

In stable magnetic structures, $\phi = \pi/2$. From the Hamiltonian [Eq.(1)] in the continuum limit, we obtain distribution of angle $\theta(x)$ of spins;

$$\theta(x) = 2\sin^{-1}\left[\mathrm{sn}\left(\frac{\sqrt{H^*}}{k}x \mid k\right)\right] + \pi, \tag{3}$$

where $\mathrm{sn}(u \mid k)$ is the Jacobi's elliptic function and k is a modulus of the elliptic function. k is determined by,

$$\frac{\pi\alpha}{4\sqrt{H^*}} = \frac{E(k)}{k}. \tag{4}$$

$E(k)$ is the complete elliptic integral of the second kind and $\alpha = \tan^{-1}(D/J)$. H^* in Eqs.(3) and (4) is a normalized applied magnetic field,

$$H^* = \frac{2\mu_B H_{\rm appl}}{a^2 S^2\sqrt{J^2+D^2}}, \tag{5}$$

where a is a lattice constant and we assume $a \sim \xi_0$ (ξ_0 is a coherence length at zero temperature). Finally, from Eqs.(2) and (3), $(\boldsymbol{H}_{\rm ext})_z$ is given by,

$$(\boldsymbol{H}_{\rm ext})_z(x) = H_0\cos\theta(x) + H_{\rm appl}. \tag{6}$$

The first term is a magnetic field from the CHM $(\boldsymbol{H}_{\rm CHM})_z$ and the second term is the homogeneous applied magnetic field. The period of the helical rotation L' is determined by,

$$L' = \frac{2kK(k)}{\sqrt{H^*}}, \tag{7}$$

where $K(k)$ is the complete elliptic integral of the first kind. Under this magnetic field $(\boldsymbol{H}_{\rm ext})_z$, we solve the Ginzburg-Landau equations;

$$\alpha|\psi|^2 + \beta|\psi|^2\psi + \frac{1}{2m^*}\left(\frac{\hbar}{i}\nabla - \frac{e^*}{c}\boldsymbol{A}\right)^2\psi = 0, \tag{8}$$

$$\mathrm{curl}(\mathrm{curl}\ \boldsymbol{A} - \boldsymbol{H}_{\rm ext}) = \frac{4\pi}{c}\boldsymbol{J} = \frac{4\pi}{c}\left\{\frac{e^*\hbar}{2m^*i}(\psi^*\nabla\psi - \psi\nabla\psi^*) - \frac{e^{*2}}{m^*c}\psi^*\psi\boldsymbol{A}\right\}, \tag{9}$$

where $\alpha = \alpha_0(T - T_c)$, T is a temperature, T_c is a critical temperature, and α_0, β are coefficients. ψ is an superconuducting order parameter, e^* is an effective charge, m^* is an effective mass, $\boldsymbol{A}$ is a magnetic vector potential, and $\boldsymbol{J}$ is a supercurrent density. When we solve these equations using the finite element method, we give the initial values of the order parameter ψ randomly and obtain several stable solutions by iterations[9].

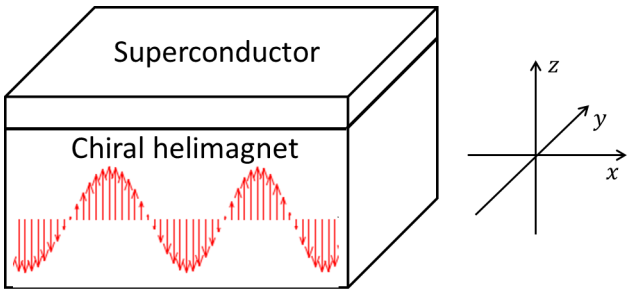

Figure 2. Chiral halimegnet (CHM) / Superconductor (SC) bilayer system.

3. Results and Discussions

We show vortex configurations in the SC under $(\boldsymbol{H}_{\rm ext})_z$ in Eq.(6). We take the Ginzburg-Landau parameter $\kappa = \lambda_0/\xi_0 = 10$ (λ_0 is a penetration length at zero temperature), the temperature $T = 0.3T_c$. The ratio between the ferromagnetic exchange interaction and the DM interaction is taken as $D/J = 0.16$, which is an experimental data of the CHM, $Cr_{1/3}NbS_2$[10]. The system sizes are $7.0L'\xi_0 \times 20\xi_0$, where L' is the helical period in Eq.(7). For $H_{\rm appl}/(\Phi_0/\xi_0^2) = 0.00$ ($\Phi_0 = h/2e$ is a quantum flux), L'/ξ_0 is approximately 39.2699.

We solve the Ginzburg-Landau equations and obtain a vortex configuration for $H_0/(\Phi_0/\xi_0^2) = 0.020$, $H_{\rm appl}/(\Phi_0/\xi_0^2) = 0.000$, which is shown in Fig.3. From the distributions of phases (b) and magnetic field (c), we find that there are two kind of vortices, which have different directions of quantum fluxes. We call these vortices up- and down-vortices, respectively. In Fig.3, we find that up- and down-vortices appear alternately. Considering a following interaction between vortices and the external magnetic field, this behavior can be explained;

$$E_{VF} = -\frac{1}{4\pi}\Phi_0 \cdot \boldsymbol{H}_{\rm ext}. \tag{10}$$

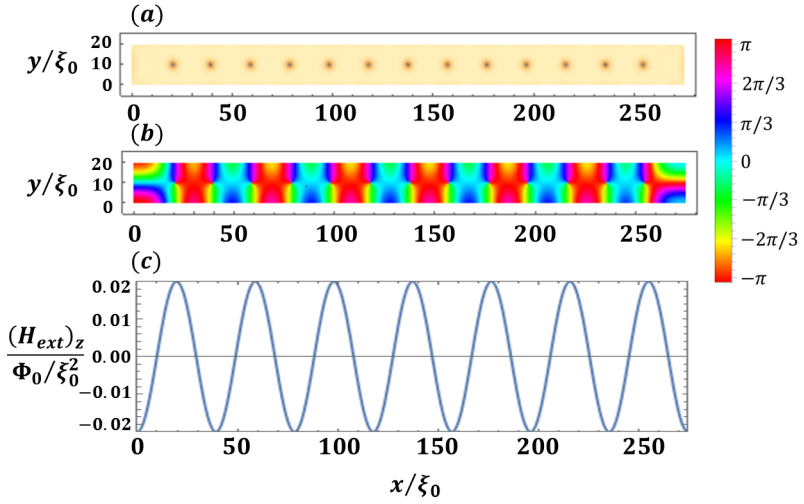

Figure 3. Distributions of (a) order parameter (vortex configuration), (b) phase, and (c) magnetic field for $H_0/(\Phi_0/\xi_0^2) = 0.020$, $H_{\rm appl}/(\Phi_0/\xi_0^2) = 0.000$.

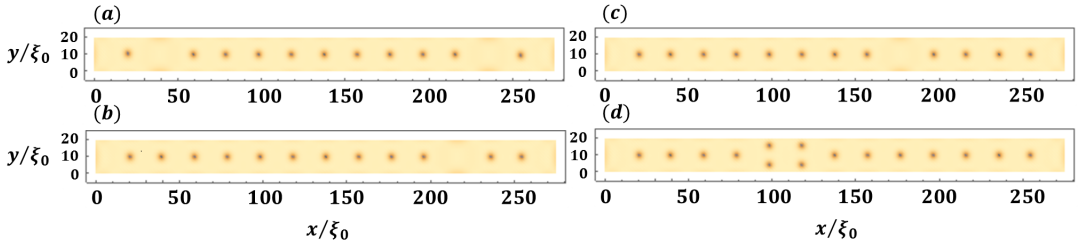

Figure 4. Vortex configurations for $H_0/(\Phi_0/\xi_0^2) = 0.020$, $H_{\rm appl}/(\Phi_0/\xi_0^2) = 0.000$.

Table 1. Free energies $\mathcal{F}$ for vortex configurations in Figs.3 and 4.

Vortex state	Free energy $\mathcal{F}$
Fig.3	4166.04062646254
Fig.4(a)	4139.90157232138
Fig.4(b)	4152.76358564515
Fig.4(c)	4152.79599929134
Fig.4(d)	4197.60960397317

When we solve the GL equations with other initial states, other vortex configurations are obtained and stable configurations are shown in Fig.4 (a) - (d). In the experiment, these vortex configurations may be found due to experimental circumstances. But, we determine the most stable vortex configuration theoretically. Therefore, we calculate the Ginzburg-Landau free energy $\mathcal{F}(\psi, \boldsymbol{A})$;

$$\mathcal{F}(\psi, \boldsymbol{A}) = \int_\Omega \left[\frac{1}{\xi(T)^2} \frac{1}{2} (|\psi|^2 - 1)^2 + |(i\nabla - \tilde{\boldsymbol{A}})\psi^2| \right] d\Omega + \kappa^2 \xi(T)^2 \int_\Omega \left| \text{curl } \boldsymbol{A} - \frac{2\pi}{\Phi_0} \right|^2 d\Omega, \quad (11)$$

where $\xi(T)$ is a coherence length and $\tilde{\boldsymbol{A}} = (2\pi/\Phi_0)\boldsymbol{A}$. These free energies are listed in Table 1. From the Table 1, vortex state in Fig.4(a) is the most stable of these states. In Fig.4(a), there are the least vortices in these states. In Fig.4(b) and (c), the numbers of vortices are same, but

vortex configurations are different. Then, free energies are different slightly. The free energy in Fig.4(d) is the largest of these states. In Fig.4(d), there are the most vortices and two vortices form pairs in the fifth- and sixth- rows from the left side.

Therefore, the most stable vortex state is Fig.4(a) for $H_0/(\Phi_0/\xi_0^2) = 0.020$ and $H_{\rm appl}/(\Phi_0/\xi_0^2) = 0.000$. If the $(\boldsymbol{H}_{\rm ext})_z$ changes, the most stable state may change from the state in Fig.4(a). When the $(\boldsymbol{H}_{\rm ext})_z$ becomes larger, the most stable state may change to states in Fig.4(b) and (c). Further $(\boldsymbol{H}_{\rm ext})_z$ becomes larger and then the vortex state in Fig.3 may become the most stable.

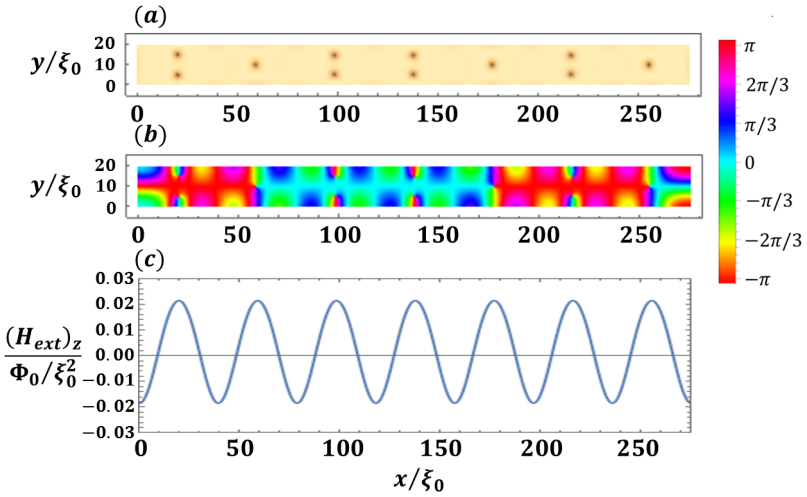

Figure 5. Distributions of (a) order parameter (vortex configuration), (b) phase, and (c) magnetic field for $H_0/(\Phi_0/\xi_0^2) = 0.020$, $H_{\rm appl}/(\Phi_0/\xi_0^2) = 0.0015$.

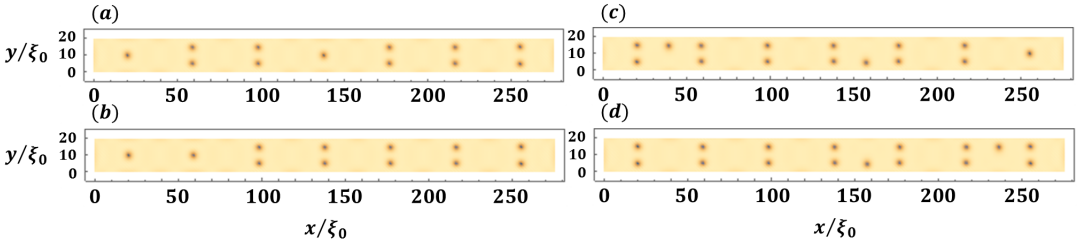

Figure 6. Vortex configurations for $H_0/(\Phi_0/\xi_0^2) = 0.020$, $H_{\rm appl}/(\Phi_0/\xi_0^2) = 0.0015$.

Next, we show effects of the CHM under the homogeneous applied magnetic field on vortex states. $H_0/(\Phi_0/\xi_0^2)$ is fixed to 0.020. The vortex configuration for $H_{\rm appl} = 0.000$ has been already shown in Figs.3 and 4. We obtain vortex configurations for $H_{\rm appl} = 0.0015$ in Figs.5 and 6. These vortex configurations result from the calculation with different initial values of the order parameter. Under the applied magnetic field ($H_{\rm appl} > 0$), the magnitude of the magnetic field in the negative magnetic field region becomes smaller. Then, the number of down-vortices decreases in Fig.6(c) and (d), or down-vortices disappear in Fig.5, 6(a) and (b). On the other hand, the magnitude of the magnetic field in the positive magnetic field region becomes larger and the number of up-vortices increases.

Table 2. Free energies $\mathcal{F}$ for vortex configurations in Figs.5 and 6.

Vortex state	Free energy $\mathcal{F}$
Fig.5	4243.23216334796
Fig.6(a)	4261.39881390694
Fig.6(b)	4261.40355039939
Fig.6(c)	4307.83875655273
Fig.6(d)	4324.99159993312

Again, we compare free energies of vortex states in Figs.5 and 6. These free energies are listed in Table 2. From the Table 2, free energies for Figs.6(c) and (d) are larger. In these vortex configurations, down-vortices remain in the second- and sixth-rows from the left side (c) and in the second- and fifth-rows from the right side (d), respectively. These down-vortices lead to the increase of free energies. On the other hand, free energies in Figs.5, 6(a) and (b) are smaller, where the down-vortices disappear. Then, we focus on the number and location of up-vortices. In Figs.6(a) and (b), the numbers of up-vortices are same, but vortex configurations are different. In particular, locations of the single vortex rows are different between these two vortex configurations. The distance between two single vortex rows in Fig.6(a) is longer than that in Fig.6(b). Then, the free energy in Fig.6(a) is slightly smaller than that in Fig.6(b). Finally, the most stable vortex state is Fig.5, where there are the least up-vortices. Similarly, the most stable state also may change from Fig.5, if the homogeneous applied magnetic field changes. From the Figs.3-6, the most stable state is controlled by the magnetic field $(\boldsymbol{H}_{\rm ext})_z$.

4. Conclusions

We have obtained vortex states in the CHM / SC bilayer systems numerically. Solving the GL equations, we found that up- and down-vortices appear in the SC. Moreover, using various initial values of the order parameter, we obtained various stable vortex configurations. Experimentally, many patterns of vortex configurations may be obtained. We compared free energies of these configurations and found the most stable state theoretically. Then, we found that the most stable state depends on the magnetic field from the chiral helimagnet and the homogeneous applied magnetic field.

Acknowledgments

This work was supported by JPSJ KAKENHI Grant Number 26400367.

References

[1] Togawa Y, Koyama T, Takayanagi K, Mori S, Kousaka Y, Akimitsu J, Nishihara S, Inoue K, Ovschinnikov A S, and Kishine J 2012 *Phys. Rev. Lett.* **108** 107202
[2] Dzyaloshinskii I E 1958 *J. Phys. Chem. Solids* **4** 241
[3] Moriya T 1960 *Phys. Rev.* **120** 91
[4] Lyuksyutov I F and Pokrovsky V L 2005 *Adv. Phys.* **54** 67
[5] Fukui S, Kato M, and Togawa Y 2015 *Physics Procedia* **65** 85
[6] Fukui S, Kato M, and Togawa Y 2016 *arXiv*:1605.05467
[7] Fukui S, Kato M, and Togawa Y 2016 *arXiv*:1605.05637
[8] Kishine J, Inoue K, and Yoshida Y 2005 *Prog. Theor. Phys. Sppl.* **159** 82
[9] Kato M, Ishida T, Koyama T, and Machida M 2013 *Superconductors-Materials, Properties and Applications, INTECH* 319-342
[10] Benjamin C, Alexander B, Nirmal G, David M, Minbhyea L 2014 *Appl. Phys. Lett.* **105** 072405